
Article:
Kilbride, R.C., Spooner, E.L.K. and Parnell, A.J. (2026) Organic photovoltaics: 30 years of the bulk heterojunction. Polymer International. ISSN: 0959-8103

https://doi.org/10.1002/pi.70097

Mini Review

Received: 1 December 2025 Revised: 26 January 2026 Published online in Wiley Online Library:

(wileyonlinelibrary.com) DOI 10.1002/pi.70097

Organic photovoltaics: 30 years of the bulk heterojunction

Rachel C. Kilbride,[a,b*] Emma L. K. Spooner[c*] and Andrew J. Parnell[d]

Abstract

Over the last 30 years, the bulk heterojunction (BHJ) has been the central architecture in organic photovoltaics (OPVs), enabling high interfacial area for efficient exciton dissociation and driving major improvements in power conversion efficiencies. This mini-review traces the development of the BHJ and the parallel evolution of OPV materials, from the first fullerene acceptors to today's highly engineered non-fullerene acceptors. Materials advances have significantly improved control over molecular packing, energetics and absorption, but have also highlighted the challenges of stabilising the inherently multicomponent BHJ morphology. We summarise current understanding of how donor–acceptor interactions, miscibility, crystallisation and film-formation kinetics shape morphology across length scales, and how these features govern charge generation, transport, recombination and operational degradation. The review also explores emerging alternatives to the conventional BHJ, including single-component and layer-by-layer systems, which challenge conventional assumptions about the need for a bicontinuous donor:acceptor network. Together, these systems reveal several ongoing challenges that need to be addressed to achieve OPVs that are not only efficient but also stable, scalable and mechanically robust.

Keywords: bulk heterojunction; energy materials; fullerene acceptors; morphology; non-fullerene acceptors; organic photovoltaics

INTRODUCTION

Organic photovoltaics (OPVs) are promising solar energy harvesting technologies that rely on the remarkable ability of conjugated, carbon-based materials to convert light into an electrical current. Unlike solar cells based on inorganic materials such as silicon, organic semiconductors offer unique advantages that include mechanical flexibility, lightweight design and importantly compatibility with large-scale solution-processing techniques.[1,2] These features make OPVs extremely attractive for a versatile range of energy applications such as lightweight portable power, building-integrated photovoltaics and indoor photovoltaics for the Internet of Things devices.[3–5]

Fundamentally, a typical OPV device consists of a solution-processed light harvesting layer comprising two materials: an electron donating semiconductor (D) and an electron accepting semiconductor (A). Upon light illumination, photons are absorbed by the donor and/or acceptor, generating tightly bound electron–hole pairs known as excitons (Fig. 1(a)). Due to the relatively low dielectric constant of organic semiconductors, these excitons must migrate to a D–A interface for charge separation to occur, producing free carriers (electrons and holes) that are subsequently transported to the electrodes and generate a photocurrent (Fig. 1(a)). A key limitation in this process is the exciton diffusion length (l_d) which defines the average distance an exciton can travel within a material before it recombines and is wasted. Whilst this parameter is material dependent, values typically range on the order of 5–20 nm.[6] As a result, only excitons generated close to an interface ($<l_d$) are likely to contribute to the photocurrent of an OPV device.

Early OPV devices employed a planar bilayer heterojunction where a donor layer and an acceptor layer are stacked to form a single, discrete interface (Fig. 1(b)).[7] Although this device architecture provided a route for exciton dissociation at the D–A interface, the limited interfacial area severely restricted the total charge generation, limiting device efficiencies to <1%. In 1995, a major breakthrough was achieved with the introduction of the bulk heterojunction (BHJ), which involves the mixing of donor and acceptor materials to form a nanoscale interpenetrating network (Fig. 1(c)).[8,9] Whilst this approach greatly increased the D–A interfacial area, it also meant that the self-assembly and resulting nanoscale morphology of the BHJ film was a decisive factor in determining the charge generation, charge transport and charge extraction.

The morphology of a BHJ blend film is determined by a complex interplay of factors, spanning both the intrinsic properties of the donor and acceptor materials and the processing conditions used

* *Correspondence to: RC Kilbride, Department of Physics, University of Warwick, Coventry, CV4 7AL, UK. E-mail: rachel.kilbride@warwick.ac.uk; or* ELK Spooner, *Photon Science Institute, University of Manchester, Oxford Road, M13 9PY, UK. E-mail: emma.spooner@manchester.ac.uk*

a *Department of Physics, University of Warwick, Coventry, UK*

b *XMaS, The UK X-ray Materials Science Facility, European Synchrotron Radiation Facility, Grenoble, France*

c *Photon Science Institute, University of Manchester, Manchester, UK*

d *School of Mathematical and Physical Sciences, University of Sheffield, Sheffield, UK*

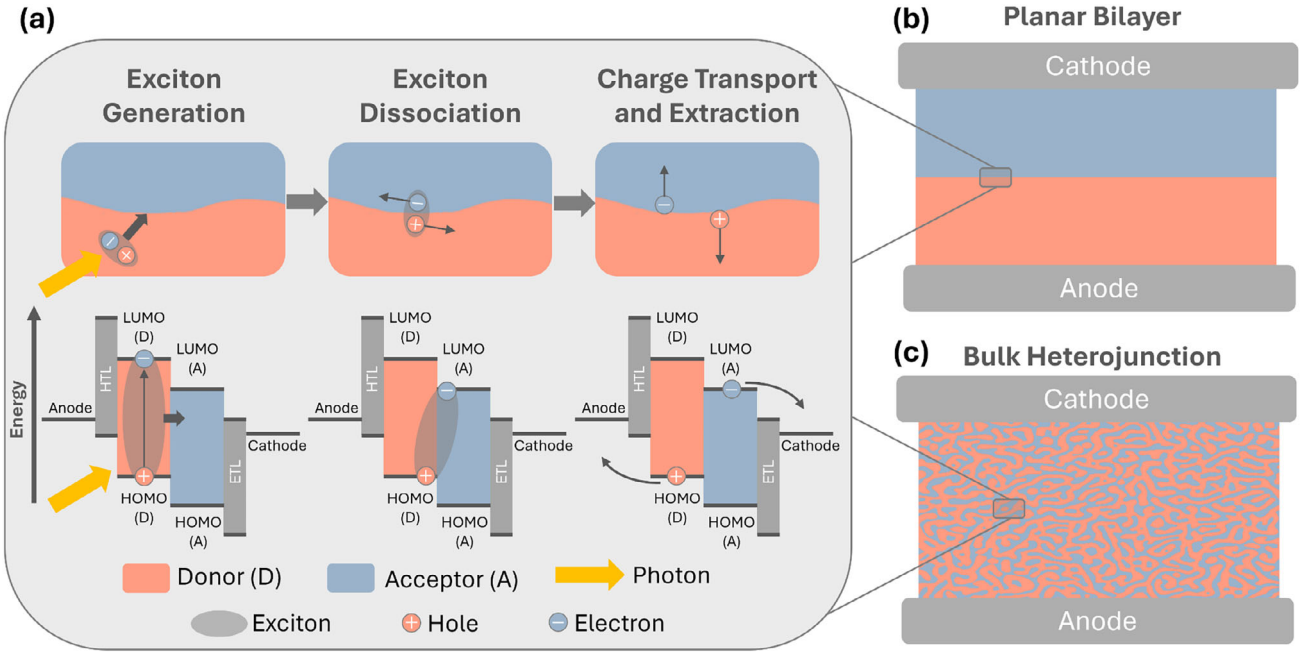

Figure 1. (a) An illustration of the key photophysical processes during photocurrent generation in (b) a planar bilayer and (c) a bulk heterojunction (BHJ) organic solar cell.

to fabricate the film. The morphology is inherently hierarchical, with characteristic length scales ranging from the ångström to the micrometre scale (Fig. 2). At the molecular scale (*ca* 0.1–5 nm), the packing and orientation of individual donor and acceptor molecules dictates the formation of larger aggregates, including J- or H-type arrangements, which influence local exciton dynamics and charge mobility.[10] At nanometre-length scales (*ca* 5–50 nm), interactions between donor and acceptor control the formation of domains, including their size, purity and degree of intermixing, all of which are critical for efficient exciton dissociation and charge percolation. On the largest scale (*ca* >50 nm), morphology is influenced by large-scale phase segregation, vertical stratification and defects, which can impact overall device performance and stability.

The formation of this hierarchical BHJ structure is governed by both thermodynamic and kinetic factors. In thermodynamic terms, the molecular interactions between donor and acceptor components (i.e. their miscibility) determine their intrinsic tendency to mix or phase separate. At the same time, kinetic factors such as solvent evaporation rate, the presence of solvent additives and processing temperature can 'freeze' the morphology into a non-equilibrium state. This kinetic quenching is a central feature of solution-processed BHJs, enabling mixed D–A regions to be attained even when thermodynamics would favour larger-scale phase separation (de-mixing). Due to the crystalline nature of most small molecule acceptors, when mixed with an amorphous donor, the BHJ will usually yield almost pure, crystalline acceptor domains and donor-rich, mixed amorphous domains.[11] Controlling this intricate, multi-scale morphology is therefore central to optimising OPV efficiency and long-term operational stability.

From a material perspective, the evolution of electron acceptors and donor polymers has played a pivotal role in shaping OPV performance. Early devices principally relied on fullerene derivatives which offered isotropic electron transport and favourable energy level alignment with many donor polymers.[13] However, fullerene acceptors suffer from inherent drawbacks, including limited

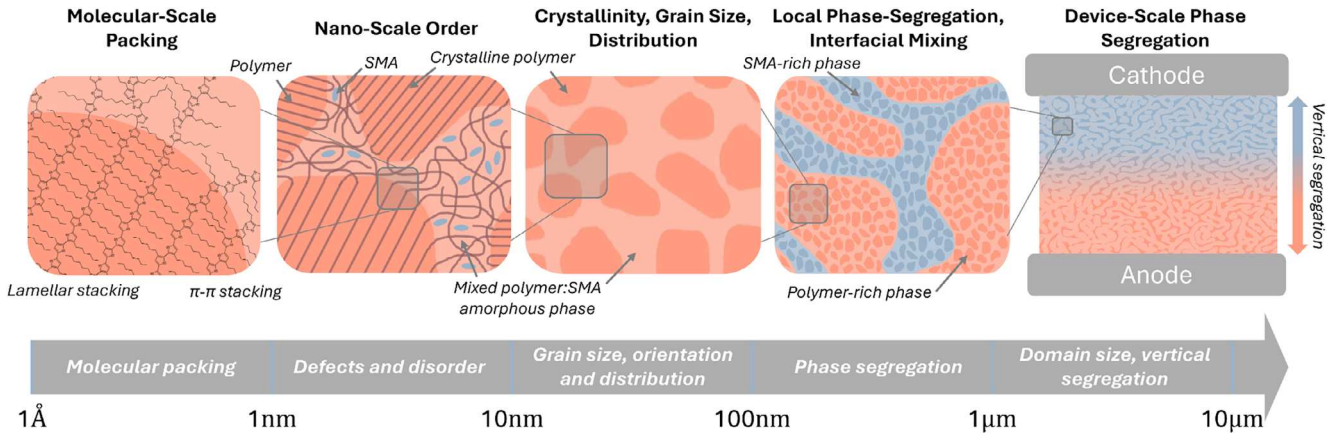

Figure 2. An illustration of the various length scales and morphological features present in a typical BHJ device layer. Adapted from Rivnay *et al*, 2012.[12]

absorption in the visible–near-infrared region and fixed energy levels. The emergence of non-fullerene acceptors (NFAs) has addressed many of these limitations by enabling greater molecular design flexibility, allowing tunable energy levels, stronger and broader absorption, and improved compatibility with donor materials.[14] As a result, NFA-based OPVs have pushed single-junction power conversion efficiencies (PCEs) beyond 20%.[15,16]

Despite this progress, long-term operational stability remains a major barrier to commercialisation.[17] BHJ films are particularly prone to morphological instabilities, often leading to unfavourable domain structures that degrade device performance and contribute to the exponential 'burn-in' efficiency loss during initial device testing.[11,18,19] These challenges have motivated extensive efforts to develop materials and processing strategies that enhance stability and preserve optimal morphology throughout device operation.

As we mark 30 years since the advent of the BHJ, this mini-review reflects on the fundamentals of BHJ morphology, traces its development from fullerenes to NFAs, examines the challenges of morphological stability, and highlights recent innovations that continue to shape the future of solution-processed OPVs.

A BRIEF HISTORY OF THE BULK HETEROJUNCTION: FROM FULLERENES TO NFAs

In this section, we provide a brief overview of BHJ OPV development, outlining the transition from fullerene- to NFA-based systems. Progress has been driven by advances in donor and acceptor materials (Fig. 3), improved device fabrication and deeper insight into the nanoscale morphology of D–A blends. Together, these advances have pushed single-junction efficiencies beyond 20%.[15,16] To understand this achievement, it is essential to revisit the key material innovations and the evolving concepts of BHJ morphology over the last 30 years.

The first BHJ device comprised a photoactive film of donor polymer poly[2-methoxy-5-(2-ethylhexyloxy)-1,4-phenylene vinylene] (MEH-PPV) and fullerene acceptor [6,6]-phenyl-C61-butyric acid methyl ester (PCBM).[8,9] This important breakthrough demonstrated that blending D–A materials together substantially increased the photocurrent relative to discrete D, A bilayers, as a greater number of excitons could dissociate at a D–A interface. However, poly(phenylene vinylene) (PPV) based OPVs often exhibited large phase-separated domains on the order of tens of nanometres, far exceeding the exciton diffusion length.[20,21] Additionally, PPV backbones showed limited crystallinity and weak π–π interactions, which translated into poor charge-carrier mobilities and restricted device performance.[22] Whilst there were some successful attempts to tune morphology through solvent selection or film processing,[23] the morphologies formed suffered from instabilities resulting in poor long-term device stability.[24]

A major leap occurred in the 2000s with the use of poly(3-alkylthiophenes), particularly regioregular poly(3-hexylthiophene-2,5-diyl) (P3HT), offering stronger absorption in the visible region and higher hole mobility compared to PPVs.[25–27] P3HT was found to self-assemble into semicrystalline lamellae, producing percolating pathways for efficient hole transport.[28,29] P3HT:PCBM blends exhibited finely interpenetrating networks (*ca* 10–20 nm), comparable to exciton diffusion lengths, and, importantly, several studies showed that the morphology was not a discrete two-phase system but also included a significant fraction of mixed D–A domains.[30,31] Morphology could be reproducibly tuned by thermal or solvent vapour annealing,[32,33] while optimisation of vertical phase segregation further improved charge extraction.[34–36] These insights underscored a broader principle that precise morphology control is essential in achieving efficient BHJ OPVs.

Optimisation of P3HT:PCBM blends resulted in a robust, semicrystalline morphology that established this system as the benchmark system for a decade of OPV research, achieving PCEs of around 5%.[37] However, PCEs plateaued due to intrinsic limitations related to the relatively narrow absorption range (*ca* 400–650 nm) of P3HT and poor overlap with the solar spectrum. This motivated the development of low-bandgap D–A copolymers in the early 2010s, which had extended absorption into the near-IR.[38,39] Early carbozole-benzothiadiazole D–A copolymers such as PCDTBT pushed efficiencies to *ca* 7%,[40–42] eventually surpassing 10% with the introduction of more successful benzodithiophene–thienothiophene (BDT-TT) copolymers such as PTB7 and PTB7-Th.[43–45] Morphological optimisation remained crucial to improving the performance of D–A copolymers systems. Thermal annealing, solvent selection and the use of high-boiling-point additives such as 1,8-diiodooctane were widely used to control film drying dynamics, D–A miscibility and the resulting BHJ morphology.[31,46,47]

Despite >10% PCE, fullerene-based OPVs plateaued due to limited energy-level tunability, narrow absorption and large voltage losses. Achieving higher PCEs relied increasingly on multicomponent strategies, such as ternary blends,[48] or the incorporation of novel additives.[49] A paradigm shift occurred in 2015 with the introduction of small molecule NFAs, based on indacenothiophene (IDT).[50–52] IDT-based NFAs are fused-ring, A-D-A type molecules that combine strong intramolecular push–pull effects and extended conjugation for broad absorption and efficient charge transport. Their highly planar backbones facilitate strong π–π stacking, while their modular 'building-block' architecture allows aggregation and packing behaviour to be tuned through side-chain and end-group modification, exemplified by the 3,9-bis(2-methylene-(3-(1,1-dicyanomethylene)-indanone))-5,5,11,11-tetrakis(4-hexylphenyl)-dithieno[2,3-d:2′,3′-d′]-s-indaceno[1,2-b:5,6-b′]dithiophene (ITIC) NFA family.[53–55] Concurrent advances in low-bandgap benzodithiophene (BDT)-benzodithiophene-dione (BDD) donor polymers such as PBDB-T and its halogenated derivatives further raised efficiencies above 13%.[56–58] The complementary tunability of ITIC-type NFAs and new donor polymers demonstrated the power of molecular engineering to control morphology and energetics, laying the groundwork for the next generation of NFAs.

Building upon the success of ITIC-type NFAs, further molecular engineering efforts led to the development of the Y-series acceptors, typified by the benchmark molecule Y6 which pushed PCEs beyond 16% in blends with PM6.[59,60] In contrast to the relatively planar architecture of ITIC derivatives, Y6 features a curved 'banana-shaped' molecular backbone with extended conjugation and flexible side chains that promote unique 3D packing motifs. This molecular curvature facilitates face-on π–π stacking, resulting in a highly ordered 'honeycomb-like' crystal structure that differs fundamentally from the lamellar packing of earlier NFAs.[60] The molecular structure of Y6 enhances charge delocalisation and provides balanced transport, while side-chain positioning and end-group fluorination enable fine control over aggregation and miscibility.[61] These features yield well-defined nanoscale domains with optimal purity and connectivity, minimising recombination

Polymer International published by John Wiley & Sons Ltd on behalf of Society of Chemical Industry.

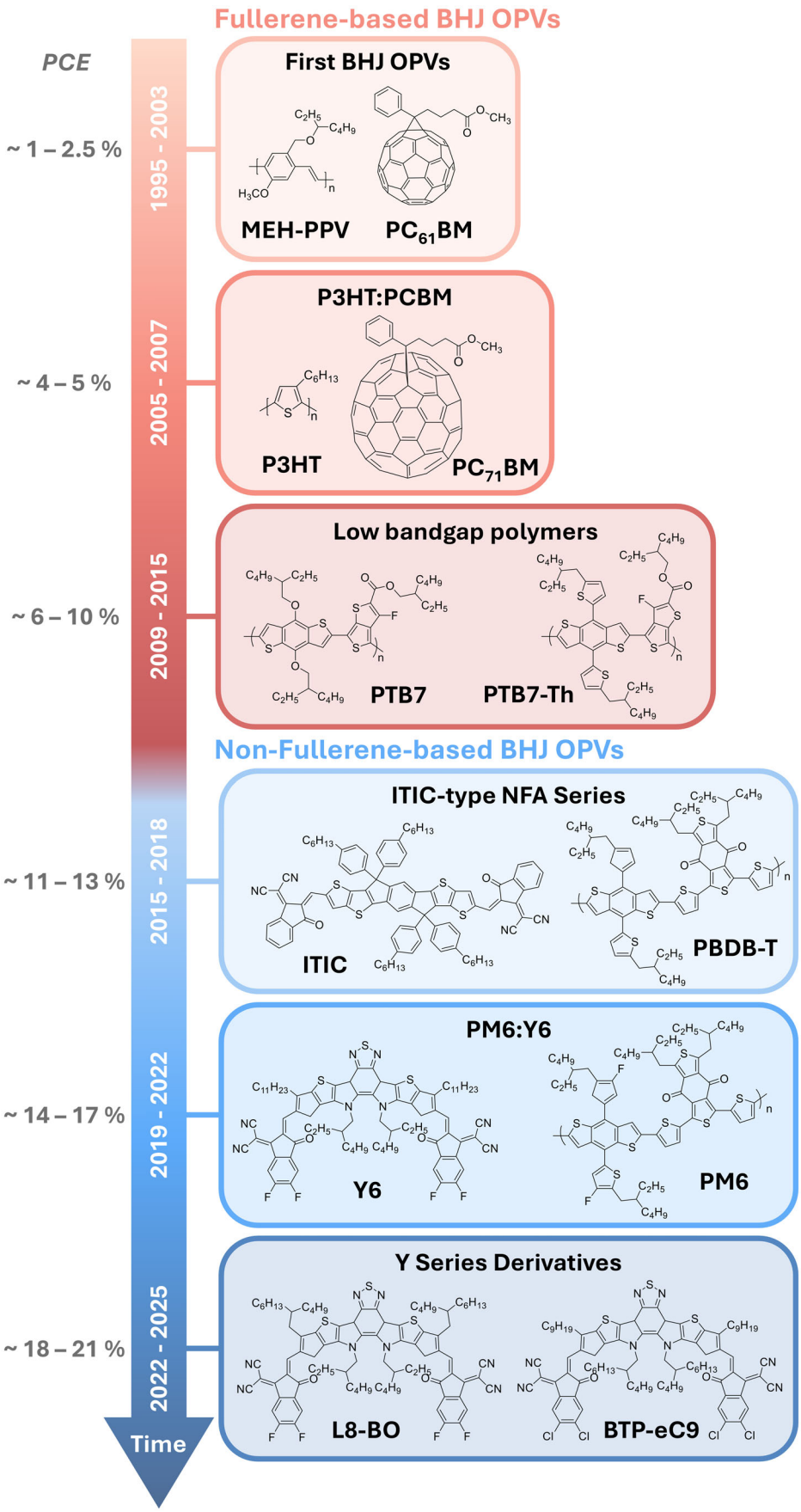

(Figure legend continues on next page.)

and energy loss. State-of-the-art OPVs now employ Y6-derived NFAs such as L8-BO and BTP-eC9, which feature subtle side-chain and end-group refinements to optimise packing, energy alignment and morphological stability, pushing efficiencies beyond 20% and approaching the practical limits of single-junction OPVs.[62,63]

MORPHOLOGICAL STABILITY

The morphological stability of an OPV device is dictated by similar factors to those that influence initial BHJ formation, namely the thermodynamic tendency to de-mix and the kinetic hindrance, or speed, of these changes. The thermodynamic miscibility between components can be described by the temperature-dependent Flory–Huggins interaction parameter ($\chi(T)$). Most high performing D–A combinations have high $\chi(T)$ values (are 'hypo-miscible'),[19] meaning that they have a high tendency to de-mix, and usually phase separate both upon initial mixing and over time.[65] This is the main route of morphological degradation in OPVs, alongside over-crystallisation of domains and de-mixing on other length scales (e.g. vertical segregation).[11]

The speed of morphological changes can be partly described by the diffusion coefficients of the constituent blend components. These have been negatively correlated with acceptor glass transition temperature (T_g) and donor elastic modulus (E_F), which are proxies for inter-molecular interactions.[19] Strong inter-molecular interactions will yield low diffusion constants, but have also been linked with hypo-miscibility,[11] illustrating the complex inter-play of kinetic and thermodynamic factors.

Exciton dissociation will occur predominantly in the mixed region of a BHJ, so the morphology of this phase (and any changes in domain composition over time) will have the greatest impact on device performance. The decrease in device efficiency as a result of morphological change will depend on the depth of the initial kinetic quench, storage temperature and how far the thermodynamic equilibrium lies from the minimum D–A mixing needed for percolation of charge carriers (percolation threshold). For example, in rare cases the BHJ is quenched at ratios higher than the percolation threshold, and de-mixing can (temporarily) increase performance due to domain purification.[11]

The relationship between the Flory–Huggins interaction parameter, morphology and stability can be described via the phase diagram shown in Fig. 4. Here $\chi(T)$ is plotted against small molecule acceptor (SMA) content in the mixed region of the film (Φ_{SMA}), with the grey line representing the acceptor content at local thermodynamic equilibrium for each χ value (known as the binodal). The formation of a single- or two-phase system is dependent on the χ value of the components and the ratio of the mixture. The phase diagram shows a typical hypo-miscible OPV, prepared at equivalent D:A ratio content, kinetically quenched to a non-equilibrium state (Q) within the percolation threshold. De-mixing towards the binodal would tend towards a lower acceptor content (M), adversely impacting performance once below the percolation threshold. The pure acceptor phase (S) and an ideal system at percolation when at equilibrium (P) are also shown.

Improving morphological stability has mostly focused on new methods to kinetically quench or hinder the BHJ long term, as improving miscibility can reduce performance.[19] These include enhanced inter-molecular interactions[66] and materials with high T_g,[67] to slow diffusion, alongside crosslinking via functional groups[68] or supramolecular assemblies to lock in optimal morphologies.[69] Careful processing can also help freeze morphologies, for example avoiding classic solvent additives with low volatility[70,71] and choosing solid additives,[72] or using a third inert polymer or compatibiliser.[73] Ternary components that can 'alloy' with one of the donor or acceptor can also help freeze morphology.[74] Other suggestions include increasing the size of the acceptor to reduce diffusion coefficients.[19,75]

BEYOND THE BULK HETEROJUNCTION

As the PCE of BHJ OPVs surpasses 20%, recent progress has shifted from molecular discovery to architectural and processing innovations that stabilise morphology and enable scalable, environmentally friendly manufacture at low cost, even if this requires discarding the traditional BHJ altogether.

Solution-processed bilayer OPVs have evolved alongside the BHJ, spanning Tang's initial publication in 1986,[7] the ubiquitous P3HT,[76] and recent ultra-high-efficiency Y-series based systems.[77] More recently, layer-by-layer (LbL) systems have emerged in which the donor and acceptor layers are deposited sequentially to form a 'pseudo' or 'quasi' BHJ where intermixing occurs post-deposition (Fig. 5).[78] This approach potentially provides greater control over interfaces and allows independent optimization of each layer and its drying kinetics through parameters such as thermal annealing, solvent choice and additives.[79,80]

The donor:acceptor interdiffusion region should be maximised for exciton dissociation, and is strongly influenced by the intrinsic chemical structure, crystallinity and miscibility of the polymer and NFA. These parameters provide greater control over the vertical morphology, in contrast to conventional BHJ systems that rely on the spontaneous formation of interpenetrating networks or kinetically trapped morphologies. *In situ* spectroscopic techniques have been used to great effect to probe the formation of the interdiffusion region, showing that the deposition of an acceptor onto a donor layer yielded a solvent-swelled polymer gel, facilitating acceptor diffusion into gel cavities.[81]

When the interdiffusion region is tuned optimally, LbL devices can achieve finely optimised charge generation, transport and extraction, reaching efficiencies that now rival record BHJ performance, with both exceeding the 20% PCE benchmark.[82]

Beyond simple efficiency, LbL devices have shown remarkable promise for scale-up of OPVs. LbL module performance has exceeded that of BHJs upon an increase in slot-die deposition speed and an increase in active area, both promising superior economic value in an industrial process.[83] Furthermore, LbL OPVs have shown superior photo and thermal stability[84] and mechanical stability[85] compared to BHJ OPVs with the former showing great promise for commercial products and the latter for flexible devices. These improvements have been attributed to a range of factors, such as reductions in non-geminate recombination, protection of the light-vulnerable acceptor layer,[86] and partially avoiding the unstable mixed phase of a hypo-miscible BHJ.[85]

(Figure legend continued from previous page.)
Figure 3. Chemical structures of selected polymers, fullerenes and NFAs that have played a pivotal role in the development of BHJ OPVs over the past 30 years along with approximate power conversion efficiencies (PCEs).[8,9,14,23,37,43,59,62–64]

Polymer International published by John Wiley & Sons Ltd on behalf of Society of Chemical Industry.

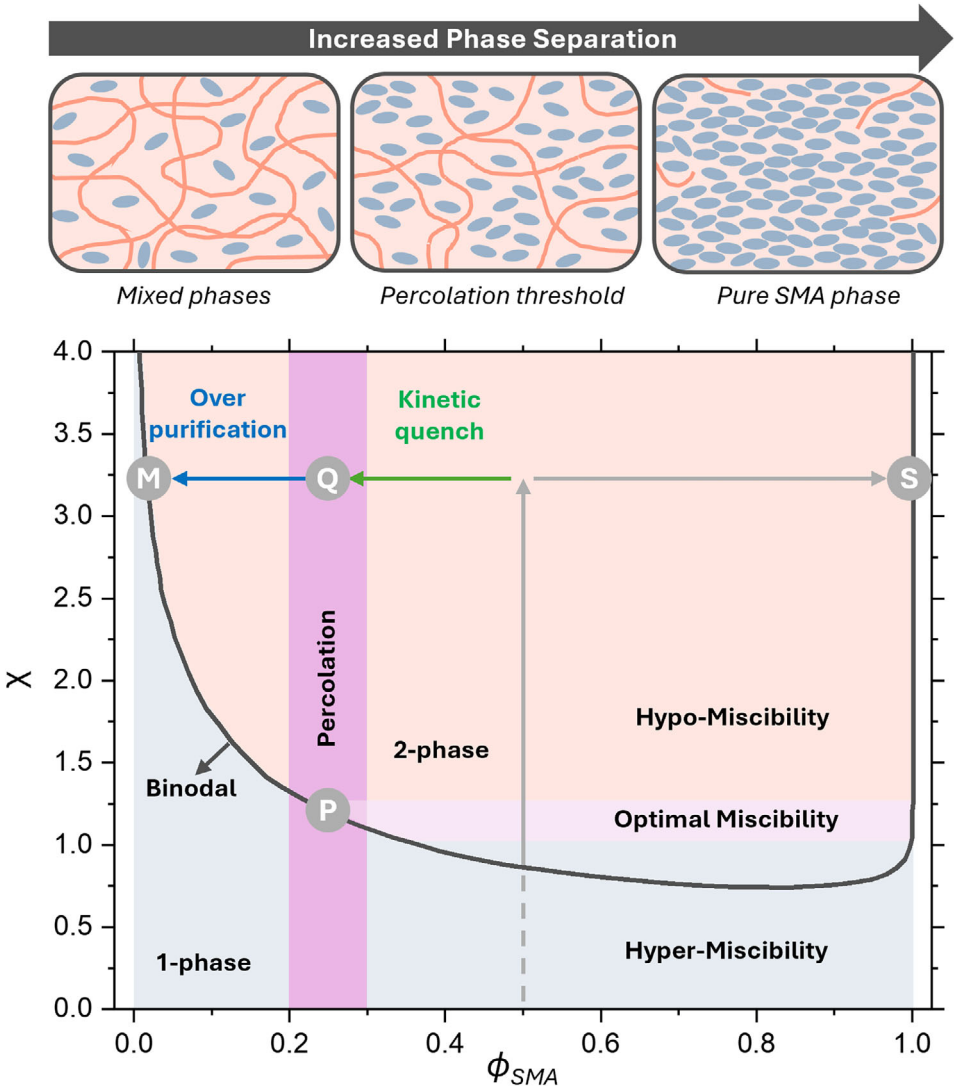

Figure 4. Phase diagram of the interaction parameter (χ) as a function of small-molecule acceptor (SMA) volume fraction (Φ_{SMA}) for a polymer:SMA blend where the binodal (grey line) separates the one- and two-phase regions. Ideal compositions of the amorphous mixed domains are typically near the percolation threshold, achievable only in hypo-miscible blends that form multiphase BHJs. Points P, Q, M and S indicate the percolation threshold in the equilibrium mixed phase (P), quenched mixed phase (Q), equilibrium mixed phase (M) and nearly pure SMA phase (S). The illustration shows the progression from a fully mixed blend, through the percolation threshold to a highly phase-separated blend containing nearly pure SMA domains. Adapted from Ghasemi *et al.*[19]

Another important development beyond BHJ-based OPVs is that of many component or 'high entropy' systems which have yielded PCEs in excess of 20%.[87] Here five or more acceptors with marginally different chemical structures are blended to increase the entropy of the active layer, yielding not only improved performance but superior stability. This stability is explained via the alloying of these marginally different components into a disordered yet thermodynamically favoured phase, a process which 'locks in' a fine-grained morphology that is resistant to further detrimental crystallisation or large-scale phase separation. Such a mixed structure is believed to reduce the probability of free electrons and holes recombining before they can be collected at the electrodes and so leads to a higher fill factor and in turn a higher overall PCE. In recent work by Zhang *et al.*,[87] the stability and high performance was attributed to reduced non-geminate recombination and preservation/freezing of the π–π stacking within the active layer, due to the alloy-like nature of the multi-acceptor phase.

The final step away from the BHJ is discarding separate donor and acceptor components all together, instead utilising so-called 'single-component' OPVs, usually from covalently bonded acceptor and donor moieties. Such an approach has yielded PCEs approaching 15%,[88] albeit at the cost of lengthy optimisation of the myriad of chemical structures available. In single-component systems the covalent bonds between donor and acceptor restrict their diffusion, avoiding the phase separation of a BHJ and yielding superior morphological, photo and thermal stability.[89,90]

Single-component OPVs are also feasible, although lower in performance, using simple high performing individual NFA molecules such as Y6.[91] Here the particularly high dielectric constant, possible direct generation of free charges, and local energetic differences may explain such behaviour. Performance of such devices is closely linked to the hole transport layer used,[92] and further developments of intrinsic charge-generating materials are likely on the horizon. Given further optimisation, this kind of

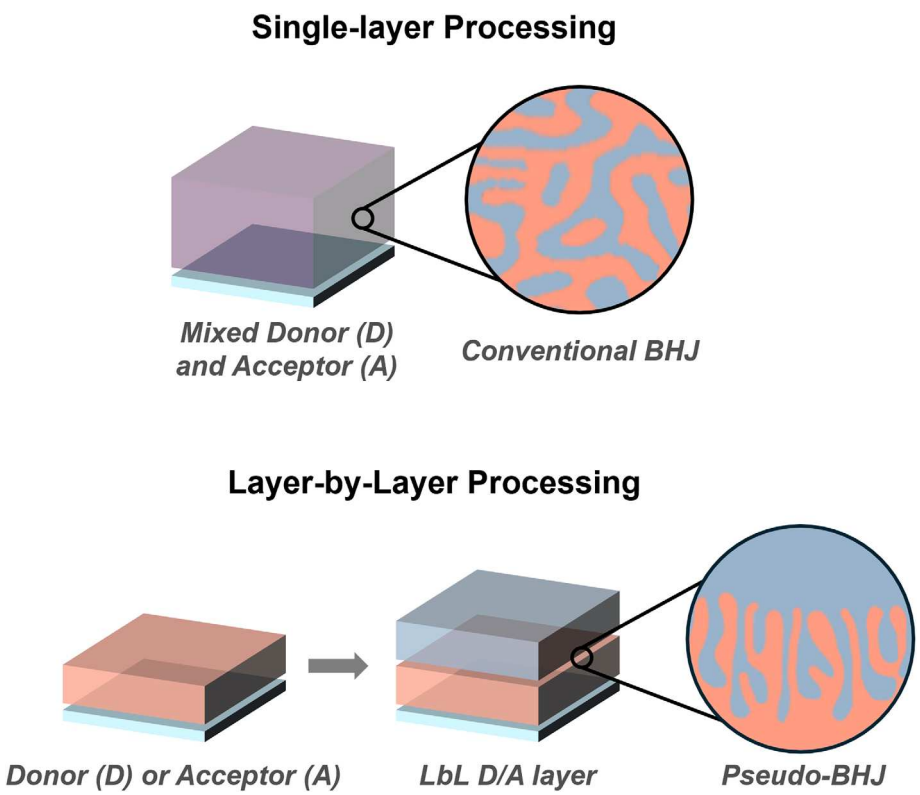

Figure 5. An illustration of single-layer processing to form conventional BHJ films and emerging layer-by-layer processing to achieve pseudo-BHJ films.

OPV may promise the simple, cheap and stable active layer of the future.

In all of these cases, fast *in situ* spectroscopic techniques have proven key to begin to unravel the unusual photophysical processes at play. Transient absorption spectroscopy in particular has been important to reveal the presence of long-range energy transfer, extending exciton diffusion lengths, in LbL systems[93] and to understand the generation of free charges and intramolecular excimer states in single-component systems.[94]

These techniques are also important when considering the future of OPVs as a whole. To improve both performance and stability, research will need to better link morphology and photophysical processes; for example using transient absorption spectroscopy to understand the relationship between crystallinity, rigidity and packing on the dimensionality and diffusion constant of excitons,[95] exciton recombination[96] and in conjunction with photoluminescence quantum yield, voltage loss.[97]

CONCLUSION AND OUTLOOK

Over 30 years since its introduction, the BHJ remains the defining architecture of OPVs, yet its limitations have become increasingly clear as the field pushes toward greater device stability and manufacturability. Emerging alternatives, particularly single component and LbL systems, offer new opportunities, but also raise fundamental questions about how photoactive structures form, operate and evolve during service. In single-component and supramolecular materials, it is still not fully understood how effective charge separation pathways arise without a discrete D–A interface, or how these internal gradients govern recombination, transport and long-term stability. Likewise, LbL approaches prompt open questions regarding vertical composition control, interdiffusion at buried interfaces and the extent to which these features improve or compromise operational stability.

Looking forward, OPV materials must achieve a delicate balance between intrinsic stability, scalable processing and mechanical durability. High T_g, rigid materials can suppress morphological diffusion but often limit flexibility, while lower T_g systems support roll to roll manufacturing yet may degrade more rapidly. The enhanced photo stability of many single-component systems suggests that both morphology and charge-carrier dynamics play crucial roles, though the underlying mechanisms remain unresolved. Addressing these challenges will be essential for transitioning OPVs from the laboratory to commercially viable technologies that are durable, efficient and scalable.

ACKNOWLEDGEMENTS

R.C.K. acknowledges the Engineering and Physical Sciences Research Council (EPSRC) for funding via grant EP/Y031962/1: XMaS: The National Material Science Beamline Research Facility at the ESRF. E.L.K.S thanks Innovate UK, the University of Manchester and Contra Vision for postdoctoral funding under Knowledge Transfer Partnership project 10030528 and Impact Acceleration Account 649.

REFERENCES

1 Lu X, Xie C, Liu Y, Zheng H, Feng K, Xiong Z *et al.*, *Nat Energy* **9**:793–802 (2024).
2 Bernardo G, Lopes T, Lidzey DG and Mendes A, *Adv Energy Mater* **11**: 2100342 (2021).
3 Jahandar M, Kim S, Kim YH and Lim DC, *Adv Energy Sustainability Res* **4**: 2200117 (2023).
4 Sha M-Z, Pu Y-J, Yin H and Hao X-T, *Org Electron* **114**:106736 (2023).

Polymer International published by John Wiley & Sons Ltd on behalf of Society of Chemical Industry.

5 Feroze S, Distler A, Dong L, Wagner M, Channa IA, Hoga F *et al.*, *Energy Environ Sci* **18**:674–688 (2025).
6 Firdaus Y, Le Corre VM, Karuthedath S, Liu W, Markina A, Huang W *et al.*, *Nat Commun* **11**:5220 (2020).
7 Tang CW, *Appl Phys Lett* **48**:183–185 (1986).
8 Yu G, Gao J, Hummelen JC, Wudl F and Heeger AJ, *Science* **270**:1789–1791 (1995).
9 Halls JJM, Walsh CA, Greenham NC, Marseglia EA, Friend RH, Moratti SC *et al.*, *Nature* **376**:498–500 (1995).
10 Li D, Zhang X, Liu D and Wang T, *J Mater Chem A* **8**:15607–15619 (2020).
11 Ghasemi M, Hu H, Peng Z, Rech JJ, Angunawela I, Carpenter JH *et al.*, *Joule* **3**:1328–1348 (2019).
12 Rivnay J, Mannsfeld SCB, Miller CE, Salleo A and Toney MF, *Chem Rev* **112**:5488–5519 (2012).
13 Lai Y-Y, Cheng Y-J and Hsu C-S, *Energy Environ Sci* **7**:1866–1883 (2014).
14 Wu X, Yang X, Chang B, Sun R and Min J, *Joule* **9**:102169 (2025). https://doi.org/10.1016/j.joule.2025.102169.
15 Chen C, Wang L, Xia W, Qiu K, Guo C, Gan Z *et al.*, *Nat Commun* **15**:6865 (2024).
16 Zhou J, Wang L, Liu C, Guo C, Chen C, Sun Y *et al.*, *J Am Chem Soc* **146**:34998–35006 (2024).
17 Riede M, Spoltore D and Leo K, *Adv Energy Mater* **11**:2002653 (2021).
18 Ye L, Hu H, Ghasemi M, Wang T, Collins BA, Kim JH *et al.*, *Nat Mater* **17**:253–260 (2018).
19 Ghasemi M, Balar N, Peng Z, Hu H, Qin Y, Kim T *et al.*, *Nat Mater* **20**:525–532 (2021).
20 Martens T, D'Haen J, Munters T, Beelen Z, Goris L, Manca J *et al.*, *Synth Met* **138**:243–247 (2003).
21 van Duren JKJ, Yang X, Loos J, Bulle-Lieuwma CW, Sieval AB, Hummelen JC *et al.*, *Adv Funct Mater* **14**:425–434 (2004).
22 Wright M, Lin R, Tayebjee MJY and Conibeer G, *Sol RRL* **1**:1700035 (2017).
23 Shaheen SE, Brabec CJ, Sariciftci NS, Padinger F, Fromherz T and Hummelen JC, *Appl Phys Lett* **78**:841–843 (2001).
24 Hoppe H and Sariciftci NS, *J Mater Chem* **16**:45–61 (2006).
25 Koezuka H, Tsumura A and Ando T, *Synth Met* **18**:699–704 (1987).
26 Padinger F, Rittberger RS and Sariciftci NS, *Adv Funct Mater* **13**:85–88 (2003).
27 Schilinsky P, Waldauf C and Brabec CJ, *Appl Phys Lett* **81**:3885–3887 (2002).
28 Li G, Shrotriya V, Huang J, Yao Y, Moriarty T, Emery K *et al.*, *Nat Mater* **4**:864–868 (2005).
29 Yang X, Loos J, Veenstra SC, Verhees WJ, Wienk MM, Kroon JM *et al.*, *Nano Lett* **5**:579–583 (2005).
30 Yin W and Dadmun M, *ACS Nano* **5**:4756–4768 (2011).
31 Hedley GJ, Ward AJ, Alekseev A, Howells CT, Martins ER, Serrano LA *et al.*, *Nat Commun* **4**:2867 (2013).
32 Verploegen E, Mondal R, Bettinger CJ, Sok S, Toney MF and Bao Z, *Adv Funct Mater* **20**:3519–3529 (2010).
33 Parnell AJ, Cadby AJ, Mykhaylyk OO, Dunbar ADF, Hopkinson PE, Donald AM *et al.*, *Macromolecules* **44**:6503–6508 (2011).
34 Campoy-Quiles M, Ferenczi T, Agostinelli T, Etchegoin PG, Kim Y, Anthopoulos TD *et al.*, *Nat Mater* **7**:158–164 (2008).
35 van Bavel S, Sourty E, de With G, Frolic K and Loos J, *Macromolecules* **42**:7396–7403 (2009).
36 Parnell AJ, Dunbar AD, Pearson AJ, Staniec PA, Dennison AJ, Hamamatsu H *et al.*, *Adv Mater* **22**:2444–2447 (2010).
37 Dang MT, Hirsch L and Wantz G, *Adv Mater* **23**:3597–3602 (2011).
38 Boudreault P-LT, Najari A and Leclerc M, *Chem Mater* **23**:456–469 (2011).
39 Dou L, Liu Y, Hong Z, Li G and Yang Y, *Chem Rev* **115**:12633–12665 (2015).
40 Blouin N, Michaud A and Leclerc M, *Adv Mater* **19**:2295–2300 (2007).
41 Park SH, Roy A, Beaupré S, Cho S, Coates N, Moon JS *et al.*, *Nat Photonics* **3**:297–302 (2009).
42 Chu T-Y, Alem S, Tsang SW, Tse SC, Wakim S, Lu J *et al.*, *Appl Phys Lett* **98**:253301 (2011).
43 He Z, Xiao B, Liu F, Wu H, Yang Y, Xiao S *et al.*, *Nat Photonics* **9**:174–179 (2015).
44 Wan Q, Guo X, Wang Z, Li W, Guo B, Ma W *et al.*, *Adv Funct Mater* **26**:6635–6640 (2016).
45 Chen J-D, Cui C, Li YQ, Zhou L, Ou QD, Li C *et al.*, *Adv Mater* **27**:1035–1041 (2015).
46 Zhang Y, Parnell AJ, Pontecchiani F, Cooper JF, Thompson RL, Jones RA *et al.*, *Sci Rep* **7**:44269 (2017).
47 Lou SJ, Szarko JM, Xu T, Yu L, Marks TJ and Chen LX, *J Am Chem Soc* **133**:20661–20663 (2011).
48 Kumari T, Lee SM, Kang S-H, Chen S and Yang C, *Energy Environ Sci* **10**:258–265 (2017).
49 Sasitharan K, Kilbride RC, Spooner ELK, Clark J, Iraqi A, Lidzey DG *et al.*, *Adv Sci* **9**:2200366 (2022).
50 Bai H, Wang Y, Cheng P, Wang J, Wu Y, Hou J *et al.*, *J Mater Chem A* **3**:1910–1914 (2015).
51 Lin Y, Zhang ZG, Bai H, Wang J, Yao Y, Li Y *et al.*, *Energy Environ Sci* **8**:610–616 (2015).
52 Lin Y, Wang J, Zhang ZG, Bai H, Li Y, Zhu D *et al.*, *Adv Mater* **27**:1170–1174 (2015).
53 Yang Y, Zhang ZG, Bin H, Chen S, Gao L, Xue L *et al.*, *J Am Chem Soc* **138**:15011–15018 (2016).
54 Lin Y, Zhao F, He Q, Huo L, Wu Y, Parker TC *et al.*, *J Am Chem Soc* **138**:4955–4961 (2016).
55 Li S, Ye L, Zhao W, Zhang S, Mukherjee S, Ade H *et al.*, *Adv Mater* **28**:9423–9429 (2016).
56 Zhao W, Li S, Yao H, Zhang S, Zhang Y, Yang B *et al.*, *J Am Chem Soc* **139**:7148–7151 (2017).
57 Zhang S, Qin Y, Zhu J and Hou J, *Adv Mater* **30**:1800868 (2018).
58 Fan Q, Zhu Q, Xu Z, Su W, Chen J, Wu J *et al.*, *Nano Energy* **48**:413–420 (2018).
59 Yuan J, Zhang Y, Zhou L, Zhang G, Yip H-L, Lau T-K *et al.*, *Joule* **3**:1140–1151 (2019).
60 Zhu L, Zhang M, Zhou G, Hao T, Xu J, Wang J *et al.*, *Adv Energy Mater* **10**:1904234 (2020).
61 Li C, Zhou J, Song J, Xu J, Zhang H, Zhang X *et al.*, *Nat Energy* **6**:605–613 (2021).
62 Chen H, Huang Y, Zhang R, Mou H, Ding J, Zhou J *et al.*, *Nat Mater* **24**:444–453 (2025).
63 Sun Y, Wang L, Guo C, Xiao J, Liu C, Chen C *et al.*, *J Am Chem Soc* **146**:12011–12019 (2024).
64 NREL, Best Research-Cell Efficiency Chart Available: https://www.nrel.gov/pv/cell-efficiency.
65 Kilbride RC, Spooner ELK, Burg SL, Oliveira BL, Charas A, Bernardo G *et al.*, *Small* **20**:2311109 (2024).
66 Wang Y, Gao H, Sun M, Lin C-T, Li H, Lin FR *et al.*, *Adv Energy Mater* **14**:2304449 (2024).
67 Zhang C, Song J, Ye L, Li X, Jee MH, Woo HY *et al.*, *Angew Chem Int Ed* **63**:e202316295 (2024).
68 Cho HW, Jee MH, Elbashier E, Kim J, Roe J, Son J *et al.*, *Adv Funct Mater* **36**:e18984 (2025). https://doi.org/10.1002/adfm.202518984.
69 Li Y, Qi F, Fan B, Liu KK, Yu J, Fu Y *et al.*, *Adv Mater* **36**:2313393 (2024).
70 Kilbride RC, Spooner ELK, Cassella EJ, O'Kane ME, Doudin K, Lidzey DG *et al.*, *ACS Appl Energy Mater* **7**:8401–8411 (2024).
71 Spooner ELK, Kilbride RC, Cai J, Shi K, MacKenzie R, Cassella EJ *et al.*, *ACS Appl Mater Interfaces* **17**:34327–34339 (2025).
72 Zhang X, Cai J, Guo C, Li D, du B, Zhuang Y *et al.*, *Small* **17**:2102558 (2021).
73 Li B, Zhang Q, Li S, Yang X, Yang F, Kong Y *et al.*, *Chem Eng J* **438**:135543 (2022).
74 Zhang K-N, Guo JJ, Zhang LJ, Qin CC, Yin H, Gao XY *et al.*, *Adv Funct Mater* **31**:2100316 (2021).
75 Chen Q, Wang Q, Meng S, Li Z, Ren Y, Bai Y *et al.*, *Adv Mater* **37**:2505735 (2025).
76 Ayzner AL, Tassone CJ, Tolbert SH and Schwartz BJ, *J Phys Chem C* **113**:20050–20060 (2009).
77 Zhu L, Zhang M, Zhou G, Wang Z, Zhong W, Zhuang J *et al.*, *Joule* **8**:3153–3168 (2024).
78 Su Y-W, Tsai C-E, Liao T-C and Wei K-H, *Sol RRL* **8**:2300927 (2024).
79 Sun R, Guo J, Sun C, Wang T, Luo Z, Zhang Z *et al.*, *Energy Environ Sci* **12**:384–395 (2019).
80 Chen Q, Bian Z, Yang Y, Cui X, Jeffreys C, Xu X *et al.*, *Angew Chem Int Ed Engl* **63**:e202405949 (2024).
81 Wang Y, Zheng X, Chen T, Wang M, Li Y, Kong Y *et al.*, *Adv Energy Mater* **16**:2403162 (2026).
82 Fu J, Li H, Liu H, Huang P, Chen H, Fong PWK *et al.*, *Nat Energy* **10**:1251–1261 (2025).
83 Sun R, Wang T, Yang X, Wu Y, Wang Y, Wu Q *et al.*, *Nat Energy* **7**:1087–1099 (2022).
84 Kumari T, Vyalih I, León Luna MÁ, Ahmed H, Ahmad M, Atajanov R *et al.*, *Cell Rep Phys Sci* **5**:102027 (2024).
85 Sun R, Guo J, Wu Q, Zhang Z, Yang W, Shi M *et al.*, *Energy Environ Sci* **12**:3118–3132 (2019).

86 Dong S, Zhang K, Xie B, Xiao J, Yip HL, Yan H *et al*., *Adv Energy Mater* **9**: 1802832 (2019).
87 Zhang M, Zhu L, Yan J, Xue X, Wang Z, Eisner F *et al*., *Joule* **9**:101851 (2025).
88 Cheng Y, Huang B, Mao Q, Huang X, Liu J, Zhou C *et al*., *Adv Mater* **36**: 2312938 (2024).
89 Liu B, Sun H, Lee JW, Jiang Z, Qiao J, Wang J *et al*., *Nat Commun* **14**:967 (2023).
90 Wu Y, Guo J, Wang W, Chen Z, Chen Z, Sun R *et al*., *Joule* **5**:1800–1815 (2021).
91 Hume PA, Price MB and Hodgkiss JM, *JACS Au* **4**:1295–1302 (2024).
92 Sharma A, Gorenflot J, Xu H, Jurado JP, Alam S, Villalva DR *et al*., *Energy Environ Sci* **18**:7610–7623 (2025).
93 Wang J, Xie Y, Chen K, Wu H, Hodgkiss JM and Zhan X, *Nat Rev Phys* **6**: 365–381 (2024).
94 Price MB, Hume PA, Ilina A, Wagner I, Tamming RR, Thorn KE *et al*., *Nat Commun* **13**:2827 (2022).
95 Cha H, Zheng Y, Dong Y, Lee HH, Wu J, Bristow H *et al*., *Adv Energy Mater* **10**:2001149 (2020).
96 Karuthedath S, Firdaus Y, Liang R-Z, Gorenflot J, Beaujuge PM, Anthopoulos TD *et al*., *Adv Energy Mater* **9**:1901443 (2019).
97 Zhu X, Gu C, Cheng Y, Lu H, Wang X, Ran G *et al*., *Adv Mater* **37**:2507529 (2025).